BULLETIN OF THE POLISH ACADEMY OF SCIENCES
TECHNICAL SCIENCES
Vol. 56, No. 3, 2008

From magnetic fluids up to complex biocompatible nanosized magnetic systems

P.C. MORAIS*

Institute of Physics, University of Brasília, Brasília DF 70910-900, Brazil

Abstract. The paper presents magnetic fluid as an excellent material platform for producing more complex magnetic drug delivery systems. In addition, the paper discusses the nanoparticle morphological (electron microscopy) and structural (X-ray diffraction) characterizations. Mössbauer spectroscopy and photoacoustic spectroscopy are revisited as key tools in the characterization of the magnetic core and diamagnetic shell of the magnetic nanoparticle, respectively.

Key words: magnetic drug delivery system, magnetic fluid, magnetoliposome, magnetic nanocapsule, magnetic nanoemulsion, Mössbauer spectroscopy, photoacoustic spectroscopy.

1. Introduction

The successful development of biocompatible nanosized magnetic material systems, in particular a magnetic drug delivery system (MDDS), requires full access to different levels of information regarding the material's properties plus "in vitro" and "in vivo" tests [1–3]. These requirements demand the joint effort of professionals with different backgrounds in unfolding the material's properties and the biological responses. Ultimately, the pre-clinical tests and the clinical trials of a new MDDS are nowadays expected to be supported by the very knowledge of the interaction between the drug and the template material that carries the drug, site-target the drug and delivers the drug. In between these two far-apart though intimately-connected ends we found the material's preparation routes and the physical and physico-chemical characterization of the drug-loaded and drug-unloaded MDDS (l-MDDS and u-MDDS). Most of the on developing MDDS, based on the platform offered by the colloidal suspension of chemically-precipitated magnetic nanoparticle, include the so-called superparamagnetic iron oxide nanoparticle (SPIO). More specifically, cubic ferrites have been used to produce most of the SPIO-based biocompatible materials [4]. Therefore, as one might expect, different experimental techniques, selected to probe the SPIO-core as well as the SPIO-shell, play a key role in helping characterizing and understand the very properties of the l-MDDS and u-MDDS. This review paper is intended to emphasize the use of the cubic ferrite-based magnetic fluid [5–7] as an extremely useful material platform in the engineering of complex biocompatible MDDS. Examples of recently developed MDDS include magnetoliposome [8], magnetic nanocapsule [9], and magnetic nanoemulsion [10]. With that purpose in mind the synthesis of the cubic ferrite-based SPIO via alkaline co-precipitation of aqueous-complexes of transition-metal ions, the morphological, the structural, the physical characterization of the as synthesized nanoparticle, and the peptization of the nanoparticle as a highly-stable magnetic fluid sample will be addressed in the paper. Besides the morphological and structural characterizations using respectively high resolution microscopy and X-ray diffraction examples of using Mössbauer spectroscopy and photoacoustic spectroscopy in probing respectively the SPIO-core and the SPIO-shell will be discussed in the paper. Indeed, applications of complex MDDS for cell-labeling (CL), photodynamic therapy (PDT), and magnetohyperthermia (MHT) of cancer cells and tissues will be mentioned in this review.

2. Magnetic fluid: the material platform for the preparation of complex biocompatible nanosized magnetic systems

Magnetic fluid (MF) is a very special colloid in which the suspended nanoparticle posses a permanent magnetic moment [11]. Considering the suspended nanoparticle ferromagnetism (for instance transition metals) and ferrimagnetism (for instance cubic ferrites) are the typical magnetic ordering observed. Nevertheless, due to the reduced particle size, typically in the range of 2–20 nm, the blocking temperature of the peptized nanoparticle occurs below or near room temperature [12]. Therefore, Néel and Brownian relaxation mechanisms compete in describing the thermal relaxation of the magnetic moment of the nanoparticle stabilized in a colloidal suspension at room-temperature [13]. Polar (water-based) as well as non-polar (hydrocarbon-based) solvents are used to peptize the magnetic nanoparticle as a stable colloidal suspension. Stable MF samples containing as much as 15% in particle volume fraction have been produced and shelved for long periods of time [14, 15]. Such a long term colloidal stability is provided by efficient particle-particle repulsion interaction. Besides the Brownian motion electrostatic and steric

*e-mail: pcmor@unb.br

repulsions are the main repulsion mechanisms providing the MF colloidal stability. Electrostatic interaction is the dominant mechanism in ionic MFs, in which the magnetic nanoparticle is suspended in low-pH (2–3) or high-pH (12–13) water-based media [14]. Steric repulsion, on the other hand, is the dominant mechanism accounting for the MF colloidal stability in hydrocarbon-based MFs, in which different non-polar solvents can be used to peptize the magnetic nanoparticle [15]. In both cases the nanoparticle surface has to be properly tailored to provide long term colloidal stability, especially in highly concentrated MF samples. In ionic MFs containing SPIO the surface polyoxy-hidroxy native molecular layer plays a key role in providing the mechanism for positively-charging the suspended nanoparticle in low-pH values [16]. In high-pH values, however, a negative surface charge density accounts for the colloidal stability in SPIO-based ionic MFs [16]. Peptization of SPIO in non-polar solvents requires a step of surface functionalization with molecules containing a hydrophobic tail facing the bulk solution, thus accounting for the steric particle-particle repulsive interaction mechanism [15]. Aqueous medium may also be used to peptize SPIO surface-coated with a molecular layer (single or multi-layered) containing a polar group in the hydrophilic tail facing the polar medium [15]. In more complex systems, such as in the biocompatible magnetic fluid (BMF), both electrostatic and steric repulsive mechanisms may take place simultaneously, providing very stable magnetic colloids at physiological condition. Nevertheless, it is worthwhile mentioning that the MF biocompatibility is assigned only after performing *in vitro* and *in vivo* tests while biocompatibility is usually a dose dependent issue [17–19]. As far as the dispersion of the single magnetic units are concerned Fig. 1a shows a mesoscopic schematic representation of how a typical freshly-synthesized MF sample might looks like in the absence of an applied magnetic field. Figure 1b shows an ideal representation of a MF sample, consisting of isolated and surface-coated nanoparticles dispersed in a carrier fluid. Indeed, Fig. 1c shows schematically how the native surface of a SPIO, obtained by the co-precipitation route in aqueous medium, might looks like at neutral pH [16]. Besides isolated nanoparticles the presence of dimers, trimers and larger agglomerates are also quoted in Fig. 1a. Experimental determination of the relative population of these magnetic units (monomer, dimer, trimer, etc) in a given MF sample can be indirectly performed using zero-field magnetic birefringence for instance [20–23]. Aging processes and/or application of external magnetic fields induce formation of chain-like structures, which had been directly visualized by cryogenic electron microscopy [24].

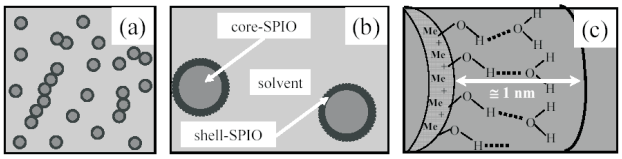

Fig. 1. Schematic representation of (a) the topological scenario of a typical magnetic fluid sample in the absence of an applied magnetic field, (b) the ideal representation of a magnetic fluid sample consisting of isolated and surface-coated nanoparticle dispersed in a carrier fluid and (c) the pH7 native surface of a metal(Me^+)-oxide nanoparticle obtained by co-precipitation in alkaline medium

The most widely used synthesis route of SPIO-based MF samples described in the literature starts with the co-precipitation of the metal ions from their aqueous salt solution using weak or strong base addition under controlled conditions. Nevertheless, fine control of the particle size and size dispersity is challenging. This is because the morphological characteristics of the end product depend upon many parameters. Among them we found the concentration of all chemical species involved (hydroxyl, metal-ions, and counter ions) in the co-precipitation reaction, the particular counter ions employed, the temperature the chemical reaction takes place, and the stirring speed. From the fundamental point of view the most intriguing dependence is the one related to the stirring speed. In the production of ionic MFs we found the average diameter of cobalt ferrite nanoparticles reducing (below 15 nm) with the increase of the stirring speed (above 1000 rpm) during the co-precipitation step. Figure 2 shows schematically a typical SPIO synthesis route employed to precipitate $CoFe_2O_4$ nanoparticles using aqueous solutions of cobalt nitrate (5 mmol/L), iron chloride (10 mmol/L) and sodium hydroxide (1 mol/L), at 95°C and under intense stirring speed. In the first step (see Fig. 2) the aqueous solution of sodium hydroxide is quickly added to the stirring solution until pH12 is reached. SPIO samples with different core-sizes can be precipitated using different stirring speeds. The as precipitated SPIO is fully-charged with a high density of negative surface charge. In the second step the supernadant is removed and nitric acid (2 mol/L) is added to the precipitate till pH3 is reached. At pH3 the SPIO is fully-charged with a high density of positive surface charge. Then, the becker containing the precipitate at low pH is left to rest overnight on top of a permanent magnet. The SPIO surface passivation is performed in the third step of the synthesis by adding hot ferric nitrate (0.5 mol/L) under continuous magnetic stirring,

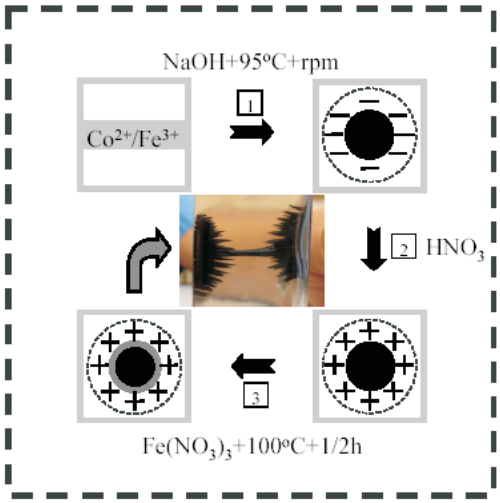

Fig. 2. Schematic representation of the alkaline chemical co-precipitation route for SPIO, with the purpose of producing stable magnetic fluid samples

for about 30 minutes. The peptization of the passivated SPIO as ionic MF sample can be accomplished in low-pH as well as in high-pH values by controlling the surface charge density while reducing the ionic strength of the aqueous medium [5–7]. In the first step of the peptization procedure triethylamine water solution (0.1 mol/L) is added dropwise to the low-pH passivated precipitate until pH6 is reached. The precipitate is then washed several times with acetone and distillated water to reduce the ionic strength of the medium. In the second step of the peptization procedure perchloric acid is added to the washed precipitate until pH2 is reached, when peptization of the SPIO as ionic MF spontaneously occurs. The picture shown in the central part of Fig. 2 was taken from a highly-concentrated ionic MF sample in the presence of two permanent magnets placed outside the wall of a glass tube containing a droplet of the sample.

One way to control the SPIO core-size is by changing the stirring speed during the first step of the synthesis. It is found that the higher the stirring speed the smaller the average mean particle diameter. However, the standard deviation associated to the lognormal particle size distribution does not change when the SPIO core-size increases by about 50% [5]. The understanding of the SPIO growth mechanism through chemical condensation reaction in aqueous solution under vigorous stirring has not been addressed in the literature, despite the huge impact it may have from the fundamental and applied viewpoints. However, the reduction of the average SPIO core-size as the stirring speed increases may indicate that the nanoparticle growth process is mainly dominated by the diffusion of the on growing nanoparticle throughout the medium instead of the diffusion of the aqueous cations into the nanoparticle surface. This seems to be an obvious conclusion, once cations are everywhere in the reaction medium while the SPIO represents a small volume fraction. Nevertheless, the distinction between normal and anomalous diffusion of the SPIO may hold the key to understand the growth process. Under normal diffusion the SPIO growth process may keep the same growth kinetics along the mean free path whereas under anomalous diffusion the growth kinetics may switch between two distinct paths, with very different growth velocities. The two distinct growth paths may occur during a sequence of short flies or during the long flies, the two scenarios typical of the anomalous diffusion [25]. Anomalous diffusion of particles inside a turbulent fluid has been already reported in the literature [26]. Under such a scenario, the SPIO growth is more likely to occur during a sequence of short flies, when space localization is much higher. As the stirring speed increases the time the SPIO spends during a sequence of short flies also increases, allowing the onset of a higher density of nucleation sites in the reaction medium, with consequent reduction of the average SPIO core-size.

Ultra-stable BMF samples based on cobalt-ferrite surface-coated with citrate anions has been prepared as described below [7]. Firstly, cobalt-ferrite is precipitated as schematically described in step-1 of Fig. 2. Then, in step-2 (see Fig. 2), the as-precipitated SPIO is washed with distillated water, following the treatment with citric acid aqueous solution (0.05 mol/L) under slight stirring for 45 min in order to promote the SPIO surface-coating. The citrate-coating step can be performed under different pH values as a strategy to fine control the SPIO citric acid surface-grafting. In step-3 (see Fig. 2) the citrate-functionalized SPIO is washed several times with acetone in order to remove any excess of citric acid and afterwards dried using a nitrogen gas flux. In the final step the dried citrate- functionalized SPIO is dispersed in distilled water and kept under slight stirring for 24 h, before centrifugation at 1000 rpm for 2 min. The obtained MF sample is adjusted to pH7 and salinity 0.9% NaCl in order to produce the highly-stable BMF sample. Similarly, following the standard procedure described in the literature [27] the meso-2,3-dimercaptosuccinic acid (DMSA) can be used to produce surface-coating maghemite (γ-Fe_2O_3) nanoparticles. As precipitated γ-Fe_2O_3 nanoparticle with an average diameter value (core sizes) of 9.3 nm was surface-coated with DMSA and used to produce stable BMF samples. The stock BMF sample can be stabilized around pH7 and salinity of 0.9% NaCl (physiological condition). With the purpose of biological applications the stock BMF sample (concentration around 10^{16} particle/mL) can be used to produce different diluted samples, quoted for instance as 1:2, 1:4, 1:20, 1:50, and 1:100. Sample 1:4, for instance, is produced by mixing one volume of the stock BMF sample with three volumes of physiological solution.

The synthesized MF samples can be further used as an exceptional and highly-flexible platform to produce more complex nanosized magnetic material systems. Starting with different MF samples [5–7] the peptized SPIO can be encapsulated as magnetoliposome [8], magnetic nanocapsule [9], or incorporated into magnetic nanoemulsion [10]. The "ex-situ" incorporation of SPIO using the MF technological platform provides full control for nanoparticle concentration in the hosting template with excellent uniformity. In addition, by controlling the chemical compatibility between the molecular-coated SPIO and the hosting matrix the protocols used for SPIO template incorporation provides the opportunity for the addition of biologically-active molecules into the end product, which can be tailored as a MDDS. Magnetic drug delivery system consisting of biocompatible magnetic fluid (BMF), magnetoliposome (ML), magnetic nanoemulsion (MNE) and magnetic nanocapsule (MNC) are presently being produced and biologically-tested worldwide [7–10].

Functionalized maghemite nanoparticles were successfully used for labeling Swiss mice erythrocytes, opening up new perspectives of biological and medical applications of MDDS, including strategies to overcome the brain blood barrier [28]. Incorporation of zinc phthalocyanine [29], pheophorbide [30] and chlorine [31] into the shell layer of a MF has been recently described. The MDDS comprising the SPIO (magnetite or maghemite) plus the photosensitizer (phthalocyanine, pheophorbide, or chlorine) was engineered to synergetically act as a dual therapeutic agent for cancer treatment, using photodynamic (PDT) and magnetohyperthermia (MHT) therapies. Likewise, zinc phthalocyanine has been incorporated into cobalt-ferrite based magnetoliposome to produce

a MDDS [10] aiming to enhance the tumor damage using PDT and MHT therapies after minimum drug administration. A new MDDS was also produced via encapsulation of zinc phthalocyanine [32] and Foscan [33] into maghemite-based magnetic nanoemulsions. Interesting aspects regarding MNE formulation are the enhanced drug solubilization, good thermodynamic stability and easily-achieved scaling up for mass production [34]. Whereas surface passivation of the peptized SPIO need to be properly addressed to prevent chemical degradation and aging effect PDT and MHT may promote phase changes of the magnetic component in a MDDS. Therefore, a more detailed investigation of the effects of SPIO surface passivation while preventing undesirable sample aging and phase changes due to illumination with visible light or thermal annealing is required to support long-term biocompatibility of a MDDS. In order to investigate the magnetic material phase stability and identify the thermally- and optically-induced production of new magnetic phases different spectroscopic techniques have been employed. Mössbauer spectroscopy for instance provides very useful information regarding material's degradation and phase transformation in SPIO-based materials. Likewise, photoacoustic spectroscopy has been recently employed for probing molecular species attached to the nanoparticle surface, thus providing valuable information regarding the aging of magnetic fluids after dilution of the stock sample by the addition of extra solvent. In the next section examples of characterization of SPIO, including sample passivation and sample aging, using transmission electron microscopy, X-ray diffraction, Mössbauer spectroscopy and photoacoustic spectroscopy, will be presented.

3. Characterization of nanosized magnetic particles in complex systems

A wide variety of experimental techniques has been used to unfold morphological, structural, magnetic and optical information of SPIO. Different optical and magneto-optical techniques have been used to investigate nanosized magnetic particles as pure powder samples, suspended as a colloid system, or dispersed in a hosting template. Among them, transmission electron microscopy (TEM), X-ray diffraction (XRD), Mössbauer spectroscopy (MS) and photoacoustic spectroscopy (PAS) were selected for presentation in this paper, emphasizing their key aspects in providing information in regard to the characteristics and properties of nanosized spinel ferrite particles.

High-resolution microscopy provides direct observation of the nanoparticle shape, average size, size dispersion and spatial distribution in hosting matrices [35–42]. Correct interpretation of all the size-dependent material properties relies on the knowledge of the morphological and topological characteristics of the sample provided by high-resolution microscopy micrographs. Figure 3 illustrates the morphological characteristics of a cobalt ferrite-based nanosized sample surface-coated with citrate. Figure 3a is a representative TEM micrograph whereas Fig. 3b shows the size-dispersity histogram (vertical columns) obtained by counting particles in the TEM micrograph. In Fig. 3b the solid line going through the experimental data represents the best curve-fitting using the log-normal distribution function, with average diameter (modal size) $D_{\mathrm{TEM}} = 7.8$ nm and size dispersity (zeroth-order logarithmic standard deviation) $\sigma = 0.18$, according to the following description of the distribution function [43]:

$$P(D) = \left(\frac{\exp(-2\sigma^2)}{D\sigma\sqrt{2\pi}}\right) \exp\{-\ln^2(D/D_{\mathrm{TEM}})/2\sigma^2\}. \quad (1)$$

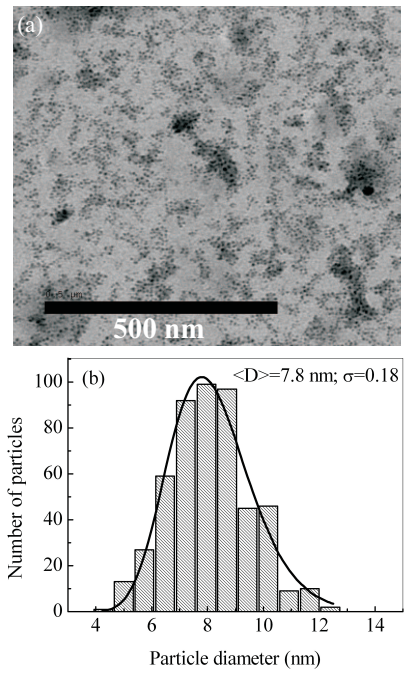

Fig. 3. Typical (a) TEM micrograph of nanosized cobalt ferrite and (b) the corresponding particle size histogram

Figure 4 shows a typical magnetic nanocomposite microsphere (200 μm average diameter) micrograph, loaded with magnetite nanoparticle. The magnetic nanocomposite microspheres were cut and imaged across the diameter using a field emission scanning electron microscope (SEM) fitted with a light element energy dispersive X-Ray (EDS) analysis. The SEM micrograph shown in Fig. 4 is a typical spherically-shaped mesoporous styrene-divinylbenzene (Sty-DVB) copolymer supporting magnetite nanoparticle. Shortly, the *in situ* synthesis of nanosized magnetite in mesoporous Sty-DVB template starts by dropping the unloaded microspheres into aqueous solution containing ferrous-ion (concentration C), which diffuses into the hosting template. Secondly, *in situ* alkaline oxidation of the adsorbed Fe^{2+}-ion in the copolymer template is performed by treating 1 g of the loaded resin with 20 mL of aqueous solution containing potassium hydroxide (0.018 mol) and sodium nitrate (1.3×10^{-3} mol), at 70°C for 15 min, under stirring. This particular chemical route of synthesizing magnetite, via partial oxidation of aqueous Fe^{2+}-ion, has been proposed by Couling and Mann [44] and recently used in the preparation of magnetite-based nanocomposites [45].

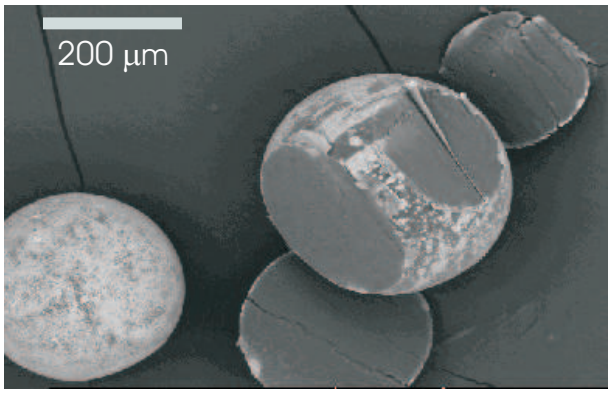

Fig. 4. Scanning electron microscopy micrograph of spherically-shaped magnetic nanocomposite consisting of magnetite nanoparticle supported in mesoporous polymeric template

X-ray diffraction (XRD) is the standard technique for probing the materials' crystal structure, providing also the average size of the nanosized particle via evaluation of the corrected full width at half height of a characteristic diffraction line [42]. Figure 5 is the XRD spectrum of a typical cobalt ferrite nanosized sample surface-coated with citrate, whose morphological characteristics were presented in Figs. 3a and 3b. The peak positions and the relative intensities of the (220), (311) and (400) XRD lines, which are the XRD fingerprint of cubic ferrites, identifies the synthesized sample as cobalt ferrite whereas the corrected full-width at half-maximum (FWHM) of the (311) reflection line provides a good estimation of the nanocrystal average diameter $D_{\mathrm{XRD}} = 11$ nm. However, the average diameter estimation needs to take into account the typical line broadening of the equipment set up, as described by the Scherrer's equation [46]:

$$D_{\mathrm{XRD}} = \frac{0.9\lambda}{B\cos\theta}, \tag{2}$$

where λ is the employed X-ray wavelength, θ is the XRD angle of the selected reflection line and B is the corrected FWHM of it, the latter defined as $\sqrt{B_S^2 - B_O^2}$, with B_S and B_O as the FWHM of the sample under investigation and a standard sample, respectively. A good standard sample for cubic ferrites is bulk crystalline silicon.

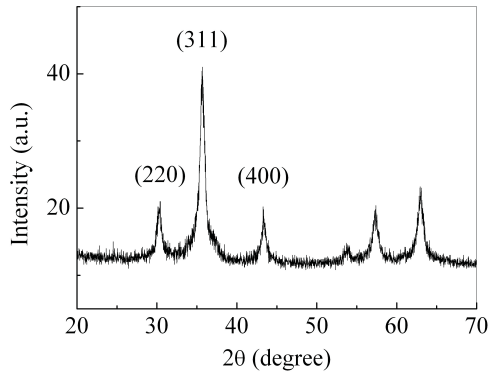

Fig. 5. Typical X-ray diffraction spectrum of nanosized cobalt ferrite particle

Mössbauer spectroscopy (MS) has long been employed for SPIO probing, in regard to their size, chemical stability, surface characteristics, cation distribution, and phase identification [47–59]. Information from the MS has been particularly useful in fine tuning the nanoparticles' synthesis protocols in order to produce materials with the desirable characteristics, such as particle size profile [5] and long term chemical stability [58]. Figure 6 shows a typical room-temperature Mössbauer spectrum of $CoFe_2O_4$ nanoparticles precipitated under a stirring speed of 2700 rpm, producing samples with 15.1 nm in average diameter and 0.30 in standard deviation, as illustrated in the inset by both the TEM micrograph and the particle diameter histogram obtained from the TEM micrograph [5]. Increasing the stirring speed up to 8100 rpm nanoparticles with 11.4 nm in average diameter were obtained while keeping about the same standard deviation [5]. The 300 K Mössbauer spectrum shown in Fig. 6 (sample consisting of 15.1 nm average diameter $CoFe_2O_4$ particles) was least square fitted using one sextet and one doublet, with the typical hyperfine parameters (isomer shift relative to natural iron of 0.47 mm/s and quadrupole splitting of 0.71 mm/s) of cobalt ferrite reported in the literature [60]. The 77 K Mössbauer spectrum still presents the typical relaxation profile, with an internal field increased by about 66 kOe. At 77 and 300 K the internal field values associated to the sextets were 489.5 and 423.7 kOe, respectively. Reduction of the internal field value was observed in both cases; as the temperature increases for all produced samples and as the stirring speed increases in all recorded temperatures. The collapsing of the internal field in both cases is typical of the superparamagnetic behavior of nanosized cobalt ferrite particles. Actually, combination of Mössbauer data with magnetization measurements (DC and AC) has been used to provide deeper insight in regard to the SPIO particle-particle interaction [61, 62] and SPIO surface effects [63, 64]. The presence of isolated or interacting SPIO particles is clearly observed in the zero-field-cooled and field-cooled magnetization curves [65, 66].

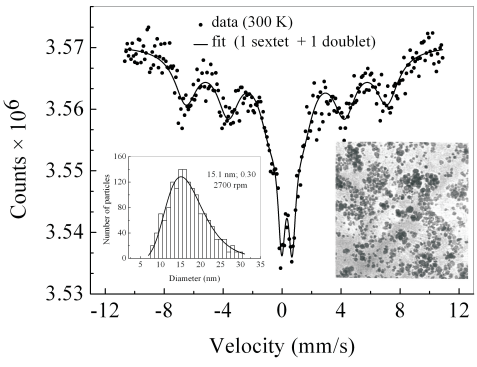

Fig. 6. Room-temperature Mössbauer spectrum of nanosized cobalt ferrite particle. The right hand-side inset is a typical transmission electron microscopy micrograph of the sample whereas the left hand-side inset is the corresponding particle size histogram

Though Photoacoustic (PA) spectroscopy is considered a well-established experimental technique only recently its

excellence in accessing information regarding the molecular species attached onto the SPIO surface has been emphasized [67–69]. Experimentally, the PA spectroscopy is based on the detection of the acoustic signal resulting from the non-radiative de-excitation processes that occur in a material system submitted to an excitation by modulated electromagnetic radiation [70]. The PA effect was discovered by Bell about 125 years ago [71], though the theoretical interpretation was given a few decades ago by Parker [72] and the applications to solid materials explored by Rosencwaig and Gersho [73]. Although PA spectroscopy has been used as a material characterization technique for over three decades [74], the technique has been only recently used in the investigation of magnetic nanoparticles peptized as MFs [75–77] or incorporated in MDDS consisting of bovine serum albumin-based nanocapsule [78]. In the conventional PA spectroscopy the sample (solid or liquid) to be investigated is placed inside a closed chamber (the photoacoustic cell) filled with a suitable gas. While modulated radiation shines onto the sample surface the generated photoacoustic signal is detected by a sensitive microphone attached to the photoacoustic cell [79]. Figure 7 shows a typical block-diagram representation of the PA experimental setup. The PA spectra are usually normalized with respect to the spectra of a highly absorbing (black) film recorded in the same wavelength range of the experiment. In our experimental setup the light from a 150 watts Xe lamp is dispersed by a 0.22 m double monochromator (Spex model 1680) and used as the variable wavelength light source in the range of 300–1000 nm. The light is chopped at a frequency of a few hertz, to improve the acoustic signal-to-noise ratio. Despite the simplicity of the PA spectroscopy the experimental data taken from the MF samples had revealed important details regarding the core nanoparticle properties, the surface nanoparticle structure, and the nanoparticle coating layer characteristics [75–77].

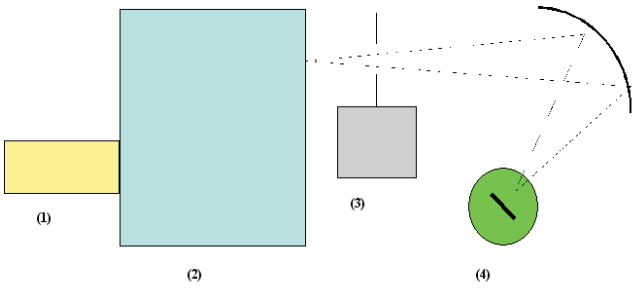

Fig. 7. Typical block-diagram of a photoacoustic spectrometer including the lamp (1), monochromator (2), chopper (3), and photoacoustic sample cell (4)

The features observed in the PA spectra of magnetic fluid samples have been described in terms of three distinct bands, namely L, S, and C [75]. Band-L, around 700 nm, has been associated to the nanoparticle surface coating layer. Therefore, band-L can be used to probe the chemical group the molecular coating species use to bind at the nanoparticle surface, indicating the surface grafting coefficient of the coating species [80]. Band-S, typically around 500 nm, is related to the modified polyoxy-hydroxy surface layer built up at the nanoparticle surface during the chemical precipitation process in aqueous medium, which is particularly enriched by hydroxyl groups. In case of metal oxide-based nanoparticles band-S can be quantitatively used to obtain the surface grafting coefficient associated to the stabilizing polyoxy-hidroxy layer [80]. Finally, band-C, observed in the low-wavelength side of the spectra (300 to 400 nm), is discussed in terms of the core size-dependence of the optical absorption [76]. Here, shifts in the band-C wavelength position are usually associated to the quantum confinement effect whereas multiplicity in the photoacoustic feature may indicate the energy level structure inside the magnetic quantum dot structure [76]. In addition, the wavelength dependence of the PA signal in the band-C region may indicate the dimensionality of the nano-sized structure [77].

Figure 8a shows a typical PA spectrum recorded from the DMSA-coated maghemite nanoparticle suspended as BMF sample (1:4 dilution). Samples containing distinct volume fraction, corresponding to the stock sample (10^{16} particle/mL) plus two diluted samples (1:2 and 1:4), were investigated. The PA spectra were recorded from the BMF samples by firstly depositing a thin liquid film on top of a polished quartz substrate and secondly drying the thin film in air at atmospheric pressure. Following the standard experimental protocol the BMF samples were enclosed in a sealed, high-performance, PA cell at atmospheric pressure, coupled to a sensitive microphone. For the three samples investigated, several PA features were observed in the wavelength range of 300 to 1000 nm. Figure 8b shows the PA spectra in the band-S region for the samples investigated (1:1, 1:2, and 1:4). Figure 8c, however, shows the PA spectra in the band-L region for all three samples investigated.

As previously reported [75, 80] the data shown in Fig. 8a–c can be analyzed in terms of three distinct bands (band-C, band-S, and band-L), in the investigation wavelength range (300 to 1000 nm). Band-C was observed around 360 nm in the BMF samples, which is about the same intensity for all samples investigated. Band-S was observed around 470 nm, which intensity reduces as the dilution of the biocompatible MF increases. Finally, in the 650 to 900 nm region, one observes the complex structure labeled band-L, which changes continuously as the dilution of the BMF proceeds. Differences and similarities of the features occurring in bands C, S, and L have been discussed as follows. As pointed out previously band-C is related to the absorption of the incident light by the core nanoparticle. We should mention that the PA signal scales with the optical absorption coefficient and, under low optical excitation intensities, the PA signal scales linearly with the optical absorption coefficient. Further, the optical absorption edge of most bulk cubic ferrite-based crystals is in the range of 300 to 400 nm [81]. At this point it is important to mention that a semiconductor quantum dot model has been successfully used to explain the charge-discharge mechanism as well as the stability of aqueous colloids based on ferrite nanoparticles [82]. Therefore, the main feature of band-C in the PA spectra shown in Fig. 8a, particularly the sharp drop

of the PA signal at decreasing wavelength, is the signature of the optical processes near the semiconductor absorption edge. We found from our PA spectra that band-C peaks at about the same wavelength for all the BMF samples investigated, for dilution is expected to cause little influence upon the energy level inside the 9.3 nm diameter quantum dot structure (core nanoparticle).

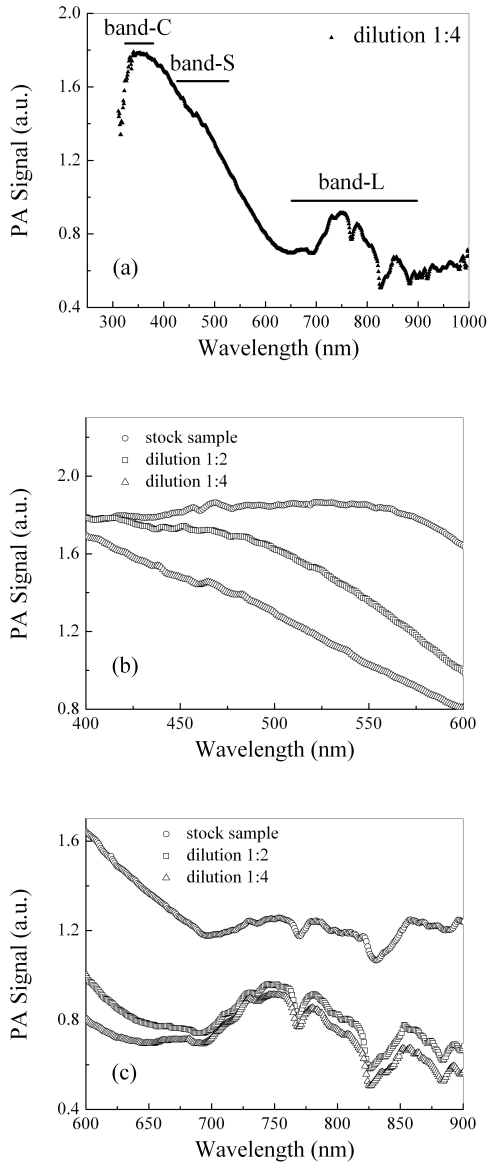

Fig. 8. Typical (a) photoacoustic spectrum of a DMSA-coated SPIO in the visible region, (b) S-band region of the stock sample and diluted samples, and (c) L-band region of the stock sample and diluted samples

Band-S is related to the polyoxy-hydroxy surface layer built up at the ferrite-based nanoparticle surface, which is particularly enriched by hydroxyl groups [16]. The shoulder around 470 nm indicates the hydroxyl-group bonded at the nanoparticle surface whereas its intensity scales with the surface hydroxyl-group grafting coefficient, similar to the observations provided by ionic MF samples [83]. The relatively lower surface-grafting coefficient associated to hydroxyl groups in the DMSA-coated BMF sample, in comparison to ionic MFs, explains the relative reduction of the PA signal intensity of the band-S feature. The interesting aspect related to the band-S provided by the spectra shown in Fig. 8b is the reduction of the shoulder intensity as the dilution of the BMF sample increases. This is a clear indication of the reduction of the surface-grafting coefficient associated to hydroxyl group. As observed in the PA spectra shown in Fig. 8c the reduction of the band-S intensity coincides with the onset of a new structure in the lower-wavelength side (around 680 nm) of band-L. Further, the peak-to-valley ratio of this new structure increases as the MF sample dilution increases. At this point it is important to mention that the features observed in both band-L and band-S are related to d-d transitions between $T_{1g} \leftrightarrow A_{2g}$ (band-S) and $T_{2g} \leftrightarrow A_{2g}$ (band-L) levels.

The explanation of the continuous change in both band-S and band-L features due to the dilution of the BMF sample, as observed in the PA spectra of Fig. 8b and c, is based on the following arguments. Disruption of longer chain-like structures into shorter ones due to sample dilution exposes the nanoparticle contact area to the solvent. It is claimed that in the as prepared BMF sample the nanoparticle contact area is surface-coated mainly by the hydroxyl-group instead of by the DMSA molecules. This is because the shorter hydroxyl-group allows efficient particle-particle coupling inside the chain-like structure with extra reduction of the free energy. On the other hand, the binding of the DMSA molecule onto the nanoparticle surface is realized via replacement of hydroxyl groups by one of the two carboxyl-groups, leaving behind the second carboxyl-group plus the two thiol-groups facing the bulk solvent. Therefore, the disruption of the chain-like structure with the consequent exposure of the nanoparticle contact area favors the substitution of the left over surface hydroxyl-groups by the nearby unbonded thiol-groups from the DMSA molecules. This model picture explains the reduction of the shoulder intensity around 470 nm as the dilution proceeds. Likewise, the proposed model picture explains the onset of the new structure in the lower-wavelength side (around 680 nm) of band-L as well as its intensity increase as the dilution proceeds. In support to this view the new structure around 680 nm appears at shorter wavelengths as compared to the typical band-L features around 780 nm and 860 nm and related to the binding of the carboxyl oxygen to the transition-metal ions at the SPIO surface. In other words, the binding of the thiol-group onto the SPIO surface via the sulfur atom wider the d-d transitions associated to the $T_{2g} \leftrightarrow A_{2g}$ levels. It is worthwhile mentioning that recent experiments, performed using different techniques, have revealed disruption of longer chain-like structures into shorter ones as a result of MF dilution. Magnetic resonance experiments performed with surface-coated MF samples have revealed that disruption of longer chain-like structures takes place upon dilution of the sample [84–86]. Also, disruption of longer chain-like structures (chain of nanoparticles) into shorter chains upon dilution of MF samples explains the birefringence signal in static magnetic birefringence measurements performed using different samples [87, 88].

4. Conclusions

This paper shows how important the Mössbauer and the Photoacoustic spectroscopies are in providing key information regarding the core and shell properties of cobalt ferrite nanoparticles designed to build complex magnetic drug delivery systems. The paper highlights the use of the magnetic fluid as an excellent material platform to encapsulate magnetic nanoparticles in the preparation of drug unloaded and drug loaded magnetoliposome, magnetic nanocapsule, and magnetic nanoemulsion. The empirical surface-passivation process of native magnetic nanoparticles and the surface-coating were taken as examples of the key information provided by both Mössbauer spectroscopy and Photoacoustic spectroscopy.

Acknowledgments. The financial support from the Brazilian Agencies MCT/CNPq, FAP-DF, and FINATEC is acknowledged. Also, acknowledgment goes to the members of the Brazilian Network on Nanobiomagnetism, particularly to E.C.D. Lima, R.B. Azevedo, Z.G.M. Lacava, A.C. Tedesco, S.W. da Silva, M.A.G. Soler, K. Skeff Neto, V.K. Garg, and A.C. Oliveira.

REFERENCES

[1] A.K. Gupta, R.R. Naregalkar, V.D. Vaidya, and M. Gupta, "Recent advances on surface engineering of magnetic iron oxide nanoparticles and their biomedical applications", *Nanomed.* 2, 23–39 (2007).

[2] L. Douziech-Eyrolles, H. Marchais, K. Herve, E. Munnier, M. Souce, C. Linassier, P. Dubois, and I. Chourpa, "Nanovectors for anticancer agents based on superparamagnetic iron oxide nanoparticles", *Int. J. Nanomed*. 2, 541–550 (2007).

[3] T. Murakami and K. Tsuchida, "Recent advances in inorganic nanoparticle-based drug delivery systems", *Mini-Rev. Med. Chem*. 8, 175–183 (2008).

[4] E. Matijevic, "Preparation and properties of uniform size colloids", *Chem. Mater*. 5, 412–426 (1993).

[5] P.C. Morais, V.K. Garg, A.C. Oliveira, L.P. Silva, R.B. Azevedo, A.M.L. Silva, and E.C.D. Lima, "Synthesis and characterization of size-controlled cobalt ferrite-based ionic ferrofluids", *J. Magn. Magn. Mater*. 225, 37–40 (2001).

[6] P.P.C. Sartoratto, A.V.S. Neto, E.C.D. Lima, A.L.C. Rodrigues de Sá, and P.C. Morais, "Preparation and electrical properties of oil-based magnetic fluids", *J. Appl. Phys*. 97, 10Q917 (2005).

[7] P.C. Morais, R.L. Santos, A.C.M. Pimenta, R.B. Azevedo, and E.C.D. Lima, "Preparation and characterization of ultra-stable biocompatible magnetic fluids using citrate-coated cobalt ferrite nanoparticles", *Thin Sol. Films* 515, 266–270 (2006).

[8] M. De Cuyper, M. Hodenius, Z.G.M. Lacava, R.B. Azevedo, M.F. Da Silva, P.C. Morais, and M.H.A. Santana, "Attachment of water-soluble proteins to the surface of (magnetizable) phospholipid colloids via NeutrAvidin-derivated phospholipids", *J. Colloid Interface Sci.* 245, 274–280 (2002).

[9] A.R. Simioni, O.P. Martins, Z.G.M. Lacava, E.C.D. Lima, B.M. Lacava, P.C. Morais, and A.C. Tedesco, "Cell toxicity studies of albumin-based nanosized magnetic beads", *J. Nanosci. Nanotechnol.* 6, 2413–2415 (2006).

[10] P.P. Macaroff, F.L. Primo, R.B. Azevedo, Z.G.M. Lacava, P.C. Morais, and A.C. Tedesco, "Synthesis and characterization of a magnetic nanoemulsion as a promising candidate for cancer treatment", *IEEE Trans. Magn.* 42, 3596–3598 (2006).

[11] B.M. Berkovsky, V.F. Medvedev, and M.S. Krakov, *Magnetic Fluids-Engineering Applications*, Oxford University Press, Oxford, 1993.

[12] J.C. Denardin, A.B. Pakhomov, A.L. Brandl, L.M. Socolovsky, M. Knobel, and X.X. Zhang, "Blocking phenomena in granular magnetic alloys through magnetization, Hall effect, and magnetoresistance experiments", *Appl. Phys. Lett.* 82, 763–765 (2003).

[13] P.C. Morais, A.L. Tronconi, F.A. Tourinho, and F. Pelegrini, "Investigation of the Brownian relaxation and hydrodynamic radius in magnetic nanoparticles", *Sol. St. Commun.* 101, 693–697 (1997).

[14] R. Massart, "Preparation of aqueous magnetic liquids in alkaline and acidic media," *IEEE Trans. Magn.* 17, 1247–1248 (1981).

[15] N. Buske, "Application of magnetite sols in environmental technology," *Progr. Colloid Polym. Sci.* 95, 175–180 (1994).

[16] P.C. Morais, S.W. da Silva, M.A.G. Soler, and N. Buske, "Raman spectroscopy in magnetic fluids", *Biomol. Eng.* 17, 41–49 (2001).

[17] A.C. Tedesco, D.M. Oliveira, Z.G.M. Lacava, R.B. Azevedo, E.C.D. Lima, and P.C. Morais, "Determination of binding constant K_b of biocompatible, ferrite-based magnetic fluids to serum albumin", *J. Appl. Phys.* 93, 6704–6706 (2003).

[18] A.C. Tedesco, D.M. Oliveira, Z.G.M. Lacava, R.B. Azevedo, E.C.D. Lima, and P.C. Morais, "Investigation of the binding constant and stoichiometry of biocompatible cobalt ferrite-based magnetic fluids to serum albumin", *J. Magn. Magn. Mater.* 272–276, 2404–2405 (2004).

[19] P.P. Macaroff, D.M. Oliveira, Z.G.M. Lacava, R.B. Azevedo, E.C.D. Lima, P.C. Morais, and A.C. Tedesco, "The effect of bovine serum albumin on the binding constant and stoichiometry of biocompatible magnetic fluids", *IEEE Trans. Magn.* 40, 3027–3029 (2004).

[20] A.F. Bakuzis, M.F. da Silva, P.C. Morais, L.S.F. Olavo, and K. Skeff Neto, "Zero-field birefringence in magnetic fluids: Temperature, particle size and concentration dependence", *J. Appl. Phys.* 87, 2497–2502 (2000).

[21] A.F. Bakuzis, M.F. da Silva, P.C. Morais, and K. Skeff Neto, "Irreversibility of zero-field birefringence in ferrofluids upon temperature reversal", *J. Appl. Phys.* 87, 2307–2311 (2000).

[22] K. Skeff Neto, A.F. Bakuzis, P.C. Morais, A.R. Pereira, R.B. Azevedo, L.M. Lacava, and Z.G.M. Lacava, "The influence of aggregates and relative permeability on the magnetic birefringence in ionic magnetic fluids", *J. Appl. Phys.* 89, 3362–3369 (2001).

[23] M.T.A. Eloi, E.C.D. Lima, A.C.M. Pimenta, R.B. Azevedo, and P.C. Morais, "Zero-field birefringence of biocompatible magnetic fluids: A concentration dependence investigation", *J. Magn. Magn. Mater.* 293, 220–223 (2005).

[24] M. Klokkenburg, B.H. Erne, J.D. Meeldijk, A. Wiedenmann, A.V. Petukhov, R.P.A. Dullens, and A.P. Philipse, "*In situ* imaging of field-induced hexagonal columns in magnetite ferrofluids", *Phys. Rev. Lett.* 97, 185702 (2006).

[25] A.S. Chaves, "A fractional diffusion equation to describe Levy flights", *Phys. Lett. A* 239, 13–16 (1998).

[26] A.J.C. Ladd, H. Gang, J.X. Zhu, and D.A. Weitz, "Time-dependent collective diffusion of colloidal particles", *Phys. Rev. Lett.* 74, 318–321 (1995).

[27] T. Goetze, C. Gansau, N. Buske, M. Roeder, P. Gornert, and M. Bahr, "Biocompatible core/shell nanoparticles," *J. Magn. Magn. Mater.* 252, 399–402 (2002).

[28] M.A.G. Soler, S.N. Bao, G.B. Alcântara, V.H.S. Tibúrcio, G.R. Paludo, J.F.B. Santana, M.H.A. Guedes, E.C.D. Lima, Z.G.M. Lacava, and P.C. Morais, "Interaction of erythrocytes with magnetic nanoparticles", *J. Nanosci. Nanotechnol.* 7, 1069–1071 (2007).

[29] P.P. Macaroff, D.M. Oliveira, Z.G.M. Lacava, E.C.D. Lima, P.C. Morais, and A.C. Tedesco, "Investigation of pheophorbide/magnetic fluid complex as a promising system for early cancer detection and treatment", *J. Appl. Phys.* 97, 10Q906 (2005).

[30] P.P. Macaroff, D.M. Oliveira, K.F. Ribeiro, A.C. Tedesco, Z.G.M. Lacava, E.C.D. Lima, and P.C. Morais, "Evaluation of new complexes of biocompatible magnetic fluid and third generation of photosensitizer useful to cancer treatment", *IEEE Trans. Magn.* 41, 4105–4107 (2005).

[31] D.M. Oliveira, Z.G.M. Lacava, E.C.D. Lima, P.C. Morais, and A.C. Tedesco, "Zinc phthalocyanine/magnetic fluid complex: a promising dual nanostructured system for cancer treatment", *J. Nanosci. Nanotechnol.* 6, 2432–2437 (2006).

[32] F.L. Primo, P.P. Macaroff, Z.G.M. Lacava, R.B. Azevedo, P.C. Morais, and A.C. Tedesco, "Binding and photophysical studies of biocompatible magnetic fluid in biological medium and development of magnetic nanoemulsion: a new candidate for cancer treatment", *J. Magn. Magn. Mater.* 310, 2838–2840 (2007).

[33] F.L. Primo, L. Michieleto, M.M.A. Rodrigues, P.P. Macaroff, P.C. Morais, Z.G.M. Lacava, M.V.L.B. Bentley, and A.C. Tedesco, "Magnetic nanoemulsions as drug delivery system for Foscan: permeation and retention in vitro assays for topical application in phtotodynamic therapy (PDT) of skin-cancer", *J. Magn. Magn. Mater.* 311, 354–357 (2007).

[34] B. Baroli, M.A. López-Quintela, M.B. Delgado-Charro, A.M. Fadda, and J.J. Blanco-Mendez, "Microemulsions for topical delivery of 8-methoxsalen", *J. Control. Release* 69, 209–218 (2000).

[35] C.E. Sjogren, C. Johansson, A. Naevestad, P.C. Sontum, K. Briley-Saebo, and A.K. Fahlvik, "Crystal size and properties of superparamagnetic iron oxide (SPIO) particles", *Magn. Res. Imaging* 15, 55–67 (1997).

[36] B.M. Lacava, R.B. Azevedo, L.P. Silva, Z.G.M. Lacava, K. Skeff Neto, N. Buske, A.F. Bakuzis, and P.C. Morais, "Particle sizing of magnetite-based magnetic fluid using atomic force microscopy: a comparative study with electron microscopy and birefringence", *Appl. Phys. Lett.* 77, 1876–1878 (2000).

[37] L.M. Lacava, R.B. Azevedo, Z.G.M. Lacava, N. Buske, A.L. Tronconi, and P.C. Morais, "Nanoparticle sizing: a comparative study using atomic force microscopy, transmission electron microscopy, and ferromagnetic resonance", *J. Magn. Magn. Mater.* 225, 79–83 (2001).

[38] P.C. Morais, R.B. Azevedo, L.P. Silva, D. Rabelo, and E.C.D. Lima, "Electron microscopy investigation of magnetite nanoparticles immersed in a polymer template", *Phys. Stat. Sol.* 187, 203–207 (2001).

[39] P.C. Morais, K. Skeff Neto, P.P. Gravina, L.C. Figueiredo, M.F. Da Silva, Z.G.M. Lacava, R.B. Azevedo, L.P. Silva, and M. De Cuyper, "Birefringence and transmission electron microscopy of monolayer and bilayer magnetoliposomes", *J. Magn. Magn. Mater.* 252, 418–420 (2002).

[40] D.K. Kim, M. Mikhaylova, Y. Zhang, and M. Muhammed, "Protective coating of superparamagnetic iron oxide nanoparticles", *Chem. Mater.* 15, 1617–1627 (2003).

[41] M. Mikhaylova, D.K. Kim, N. Bobrysheva, M. Osmolowsky, V. Semenov, T. Tsakalados, and M. Muhammed, "Superparamagnetism of magnetite nanoparticles: dependence on surface modification", *Langmuir* 20, 2472–2477 (2004).

[42] A.S. de Menezes, C.M.R. Remédios, J.M. Sasaki, L.R.D. da Silva, J.C. Goes, P.M. Jardim, and M.A.R. Miranda, "Sintering of nanoparticles of alpha-Fe_2O_3 using gelatin", *J. Non-Cryst. Sol.* 353, 1091–1094 (2007).

[43] B. Payet, D. Vincent, L. Delaunay, and G. Noyel, "Influence of particle size distribution on the initial susceptibility of magnetic fluids in the Brown relaxation range", *J. Magn. Magn. Mater.* 186, 168–174 (1998).

[44] S.B. Couling and S. Mann, "The influence of inorganic-phosphate on the crystallization of magnetite (Fe_3O_4) from aqueous-solution", *J. Chem. Soc. Chem. Commun.* 23, 1713–1715 (1985).

[45] P.P.C. Sartoratto, K.L.Caiado, R.C. Pedroza, S.W. da Silva, and P.C. Morais, "The thermal stability of maghemite-silica nanocomposites: an investigation using x-ray diffraction and Raman spectroscopy", *J. Alloy Compd.* 434–435, 650–654 (2007).

[46] B.D. Cullity, *Elements of X-ray Diffraction*, Addison-Wesley, London, 1978.

[47] H. Pardoe, W. Chua-Anusorn, and T.G. St Pierre, "Structural and magnetic properties of nanoscale iron oxide particles synthesized in the presence of dextran or polyvinyl alcohol", *J. Magn. Magn. Mater.* 225, 41–46 (2001).

[48] D. Rabelo, E.C.D. Lima, A.C. Reis, W.C. Nunes, M.A. Novak, and P.C. Morais, "Preparation of magnetite nanoparticles in mesoporous copolymer template", *Nano Lett.* 1, 105–108 (2001).

[49] D. Rabelo, V.J. Silva, E.F.C. Alcantara, L.C. Faria, G.A.V. Martins, V.K. Garg, A.C. Oliveira, and P.C. Morais, "Fe^{2+} and Fe^{3+} adsorption on 2-vinylpyridine-divinylbenzene copolymers and acrylonitrile-methylmethacrylate-divinylbenzene terpolymers", *J. Appl. Polym. Sci.* 89, 3905–3912 (2003).

[50] M. Mikhaylova, Y.S. Jo, D.K. Kim, N. Bobrysheva, Y. Anderson, T. Eriksson, M. Osmolowsky, V. Semenov, and M. Muhammed, "The effect of biocompatible coating layers on magnetic properties of superparamagnetic iron oxide nanoparticles", *Hyperfine Int.* 156, 257–263 (2004).

[51] D. Rabelo, E.C.D. Lima, N. Tavares Filho, F.Q. Soares, L.C. Faria, F. Pelegrini, O. Silva, A.C. Oliveira, V.K. Garg, and P.C. Morais, "Synthesis of manganese ferrite nanoparticles in macroporous styrene-divinylbenzene copolymer", *J. Magn. Magn. Mater.* 272/276, 1205–1206 (2004).

[52] V.K. Garg, A.C. Oliveira, M. Wagener, N. Buske, and P.C. Morais, "Mössbauer study of iron-nitride-based magnetic fluid", *J. Magn. Magn. Mater.* 272/276, 2326–2327 (2004).

[53] A. Sinha, S. Nayar, B.K. Nath, D. Das, and P.K. Mukhopadhyay, "Magnetic field induced synthesis and self-assembly of super paramagnetic particles in a protein matrix", *Colloids Surf. B: Biointerfaces* 43, 7–11 (2005).

[54] A.D. Arelaro, A.L. Brandl, E. Lima Jr., L.F. Gamarra, G.E.S. Brito, W.M. Pontuschka, and G.F. Goya, "Interparticle interactions and surface contribution to the effective anisotropy in biocompatible iron oxide nanoparticles used for contrast agents", *J. Appl. Phys.* 97, 10J316 (2005).

[55] N.K. Prasad, D. Panda, S. Singh, M.D. Mukadam, S.M. Yusuf, and D.J. Bahadur, "Biocompatible suspension of nanosized gamma-Fe_2O_3 synthesized by novel methods", *J. Appl. Phys.* 97, 10Q903 (2005).

[56] M.A.G. Soler, S.W. da Silva, V.K. Garg, A.C. Oliveira, R.B. Azevedo, A.C.M. Pimenta, E.C.D. Lima, and P.C. Morais, "Surface passivation and characterization of cobalt-ferrite nanoparticles", *Surf. Sci.* 575, 12–16 (2005).

[57] F. Nakagomi, S.W. da Silva, V.K. Garg, A.C. Oliveira, P.C. Morais, A. Franco Jr., and E.C.D. Lima, "The influence of cobalt population on the structural properties of $Co_xFe_{3-x}O_4$", *J. Appl. Phys.* 101, 09M514 (2007).

[58] M.A.G. Soler, E.C.D. Lima, S.W. da Silva, T.F.O. Melo, A.C.M. Pimenta, J.P. Sinnecker, R.B. Azevedo, V.K. Garg, A.C. Oliveira, M.A. Novak, and P.C. Morais, "Aging investigation of cobalt ferrite nanoparticles in low pH magnetic magnetic fluid", *Langmuir* 23, 9611–9617 (2007).

[59] M.A.G. Soler, G.B. Alcantara, F.Q. Soares, W.R. Viali, P.P.C. Sartoratto, J.R.L. Fernandez, S.W. da Silva, V.K. Garg, A.C. Oliveira, and P.C. Morais, "Study of molecular surface coating on the stability of maghemite nanoparticles", *Surf. Sci.* 601, 3921–3925 (2007).

[60] H.R. Rechenberg and F.A. Tourinho, "Mossbauer spectroscopic characterization of manganese and cobalt ferrite ferrofluids", *Hyperfine Int.* 67, 627–631 (1991).

[61] S. Morup, F. Bodker, P.V. Hendriksen, and S. Linderoth, "Spin-glass-like ordering of the magnetic moments of interacting nanosized maghemite particles", *Phys. Rev. B* 52, 287–294 (1995).

[62] J.L. Dormann, F. D'Orazio, F. Lucari, E. Tronc, P. Prene, J.P. Jolivet, D. Fiorani, R. Cherkaoui, and M. Nogues, "Thermal variation of the relaxation time of the magnetic moment of γ-Fe_2O_3 nanoparticles with interparticle interaction of various strengths", *Phys. Rev. B* 53, 14291–14297 (1996).

[63] T. Ninjbadgar, S. Yamamoto, and T. Fukuda, "Synthesis and magnetic properties of the γ-Fe_2O_3/poly-(methyl methacrylate)-core/shell nanoparticles", *Sol. St. Sci.* 6, 879–885 (2004).

[64] P.P. Vaishnava, U. Senaratne, E.C. Buc, R. Naik, V.M. Naik, G.M. Tsoi, and L.E. Wenger, *Phys. Rev. B* 76, 024413 (2007).

[65] M. Knobel, W.C. Nunes, H. Winnischofer, T.C.R. Rocha, L.M. Socolovsky, C.L. Mayorga, and D. Zanchet, "Effects of magnetic interparticle coupling on the blocking temperature of ferromagnetic nanoparticle arrays", *J. Non-Cryst. Sol.* 353, 743–747 (2007).

[66] E. Mosiniewicz-Szablewska, M. Safarikova, and I. Safarik, "Magnetic studies of ferrofluid-modified spruce sawdust", *J. Phys. D: Appl. Phys.* 40, 6490–6496 (2007).

[67] J.G. Santos, L.B. Silveira, A.C. Oliveira, and P.C. Morais, "Use of the photoacoustic spectroscopy in the investigation of biocompatible magnetic fluids", *J. Phys. IV* 125, 27–30 (2005).

[68] P.C. Morais, L.B. Silveira, J.G. Santos, A.C. Oliveira, A.L. Tronconi, R.L. Santos, E.C.D. Lima, J.M. Marchetti, and A.C. Tedesco, "Use of the photoacoustic spectroscopy for surface characterization of nanometer-sized cobalt-ferrite particles", *IEEE Trans. Magn.* 41, 3382–3384 (2005).

[69] S.R. Avelino, F.M.L. Oliveira, A.C. Oliveira, and P.C. Morais, "Use of the photoacoustic spectroscopy in the investigation of the dilution process in surface-coated nanoparticles", *J. Non-Cryst. Sol.* 352, 3692–3696 (2006).

[70] A. Rosencwaig and A. Gersho, "Photoacoustic effect with solids-Theoretical treatment", *Science* 190, 556–557 (1975).

[71] A.G. Bell, "Upon the production of sound by radiant energy", *Am. J. Sci.* 20, 305–324 (1980).

[72] J.G. Parker, "Optical-absorption in glass-investigation using an acoustic technique", *Appl. Opt.* 12, 2974–2977 (1973).

[73] A. Rosencwaig and A. Gersho, "Theory of acoustic effect with solids", *J. Appl. Phys.* 47, 64–69 (1976).

[74] A. Rosencwaig, *Photoacoustic and photoacoustic spectroscopy*, John Wiley, London, 1980.

[75] A.C. Oliveira, A.L. Tronconi, N. Buske, and P.C. Morais, "Photoacoustic spectroscopy of magnetic fluids", *J. Magn. Magn. Mater.* 252, 56–58 (2002).

[76] P.C. Morais, A.C. Oliveira, A.L. Tronconi, C. Gansau, T. Goetze, and N. Buske, "Photoacoustic spectroscopy: A promising technique to investigate magnetic fluids", *IEEE Trans. Magn.* 39, 2654–2656 (2003).

[77] P.C. Morais, A.L. Tronconi, A.C. Oliveira, R.L. Santos, and E.C.D. Lima, "Investigation of the size-effect of cobalt-ferrite nanoparticles using photoacoustic spectroscopy", *J. Phys. IV* 125, 505–508 (2005).

[78] L.B. Silveira, J.G. Santos, A.C. Oliveira, B.M. Lacava, A.C. Tedesco, and P.C. Morais, "Photoacoustic investigation of maghemite-based BSA nanocomposite", *Eur. J. Phys.* 153, 357–360 (2008).

[79] A. Rosencwaig, *Optoacoustic Spectroscopy and Detection*, Academic Press, 1977.

[80] A.L. Tronconi, A.C. Oliveira, E.C.D. Lima, and P.C. Morais, "Photoacoustic spectroscopy of cobalt ferrite-based magnetic fluids", *J. Magn. Magn. Mater.* 272–276, 2335–2336 (2004).

[81] Y.M. Chiang, D. Birnie III, and W.D. Kingery, *Physical Ceramics: Principles for Ceramic Science and Engineering*, John Wiley, London, 1997.

[82] Fanyao Qu and P.C. Morais, "Oxide semiconductor nanoparticle in aqueous medium: a surface charge density investigation", *J. Phys. Chem. B* 104, 5232–5236 (2000).

[83] P.C. Morais, A.L. Tronconi, and A.C. Oliveira, "Use of the photoacoustic spectroscopy in the investigation of ionic magnetic fluids", *Eur. Cells and Mater.* 3 (S2), 19–21 (2002).

[84] P.C. Morais, G.R.R. Gonçalves, K. Skeff Neto, F. Pelegrini, and N. Buske, "Study of particle-particle interaction in magnetic fluids using magnetic resonance", *IEEE Trans. Magn.* 38, 3225–3227 (2002).

[85] L.B. Silveira, J.G. Santos, F. Pelegrini, C. Gansau, N. Buske, and P.C. Morais, "Magnetic resonance study of zero-field-frozen magnetite-based biocompatible magnetic fluid", *IEEE Trans. Magn.* 39, 2642–2644 (2003).

[86] G.R.R. Gonçalves, A.F. Bakuzis, K. Skeff Neto, F. Pelegrini, and P.C. Morais, "Magnetic resonance investigation of the particle-particle equilibrium distance within small agglomerates in magnetic fluids", *J. Magn. Magn. Mater.* 289, 142–145 (2005).

[87] A.F. Bakuzis, K. Skeff Neto, L.P. Silva, R.B. Azevedo, and P.C. Morais, "Experimental evidence of monomer contribution to the static magnetic birefringence in magnetic fluids", *J. Appl. Phys.* 90, 891–895 (2001).

[88] A.R. Pereira, G.R.R. Gonçalves, A.F. Bakuzis, P.C. Morais, R.B. Azevedo, and K. Skeff Neto, "Magnetic birefringence in copper and zinc ferrite-based ionic magnetic fluids", *IEEE Trans. Magn.* 37, 2657–2659 (2001).